ACS OMEGA

Open Access

http://pubs.acs.org/journal/acsodf

Article

WO_3 as an Electron Exchange Matrix: A Novel and Efficient Treatment Method for Nitro Compounds

Lior Carmel, Shiran Aharon, Dan Meyerstein, Yael Albo, Lonia Friedlander, Dror Shamir,* and Ariela Burg*

Cite This: *ACS Omega* 2025, 10, 10878−10890

Read Online

ACCESS | Metrics & More | Article Recommendations | Supporting Information

ABSTRACT: To minimize the use of the chemicals that have traditionally been needed to treat toxic organic compounds, a WO_3 electron exchange matrix (EEMWO_3), which requires fewer chemical solvents in line with green chemistry engineering principles, was developed for waste degradation. The EEMWO_3 was tested for its ability to remove 4-nitrophenol and 2-nitrophenol, which were chosen as models for common oxidizing toxic compounds. The nitrophenol was added in an initial amount of 7.19×10^{-5} mol, which is a larger concentration than that reported to cause health problems. The conversion values were ∼(10−50)%, depending on the type of EEMWO_3 and on the substrate used. Ca. 10% of the WO_3 units in the matrix were observed to be reduced by BH_4^- to W(V), a value that is orders of magnitude better than that previously reported for EEM. The results indicate that the structure and the surface area of the EEMWO_3 are important parameters in the degradation process. The monoclinic hydrotungstite ($WO_2(OH)_2 \cdot H_2O$) was the reactive species. The same parameters also affected the recyclability of the process, and three cycles were possible with the commercial WO_3. The tungsten oxide functioned as an active EEM without an entrapped redox species and as a skeleton, indicating that one does not have to worry about the number of active species that can be entrapped in the matrix. It can be concluded that EEMWO_3 is an efficient treatment method for toxic, oxidizing organic compounds and that it is a greener method whose use requires fewer chemicals than conventional methods.

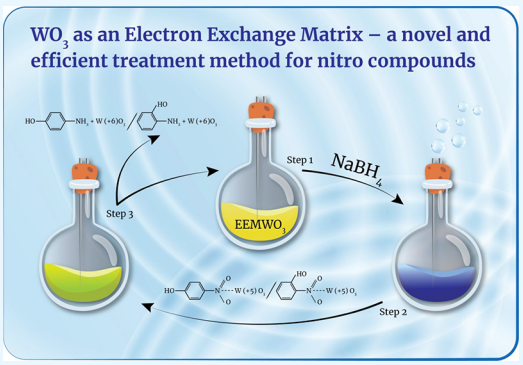

1. INTRODUCTION

The electron exchange columns (EECs) introduced in the 1950s by Cassidy[1] comprised a solid packing matrix with a bound redox agent that can oxidize or reduce one or more substrates that flow through the column without releasing the entrapped redox moiety to the solution.[1−4] Although the redox system designed by Cassidy was fundamentally unstable, the entrapment behavior exhibited by EECs can facilitate the heterogenization and performance under a flow condition of useful redox reactions that are relevant to a broad range of industrial and environmental remediation processes.[2−5] The development of highly active but stable EECs for heterogeneous redox reactions will streamline several industrial processes, thus bringing them in line with the green chemistry principles of reductions in the amount of energy needed to drive the process and in the reliance on solvents. In addition, it will also enable flexible chemical manufacturing based on customer demand, an emerging feature of the new chemical industry. The chemical industry could produce many environmental pollutants such as heavy metals,[6−8] spilled oils,[6] and organic compounds.[9−14] Halogenated organic compounds,[15−21] nitroaromatic compounds,[22−30] azo dyes,[22,31−36] and inorganic pollutants such as bromate,[4,37,38] nitrate[39−42] and nitrophenols[43−46] can be treated by photocatalytic degradation and redox reactions to obtain environmentally safe products.

Ideally suited to the field of green chemistry, EECs exploit redox reagents that are immobilized within the columns, and as such, they do not contaminate the redox product. They eliminate the need for the typically used, energy-intensive separation processes; in some cases, no solvents are required.[2−5,47,48] The heterogeneous electron transfer process will thus enable pollutant degradation without any need for a separation step. Efficient EECs could thus treat pollutants via an environmentally benign process that does not generate secondary pollutants and that meets the requirements of a green treatment.[4,47] Recently, Cohen et al.[47] found that the sol−gel electron exchange matrix (EEM, i.e., the solid packing matrix of the EEC) plays a dual role as the host of the redox species and as an oxidant species itself that is involved in the

Received: September 14, 2024
Revised: February 26, 2025
Accepted: March 3, 2025
Published: March 13, 2025

oxidation process of para chloro aniline to reduce its concentrations in wastewater streams.[47]

In the current study, to develop greener EEMs that require significantly fewer chemicals for their operation, thereby meeting green chemistry engineering principles, we prepared sol−gel matrices based on tungsten oxides (WO_3), which have attracted increased attention for their applicability in organic synthesis, photocatalysis, and electrochemistry.[49−52] In most cases, WO_3 has been widely used as a catalyst in photocatalytic applications[53−55] (a band gap of 2.5−2.8 eV[56]). However, the structure and synthesis of WO_3 catalysts are complex due in part to the need to combine the WO_3 in composite materials in the final catalytic structure to increase its catalytic activity. For example, WO_3/Ag_2CO_3,[57] WO_3/TiO_2 nanofibers,[58] and ZIF67/N,P-WO_3[53] were used to degrade rhodamine B, methylene blue, and levofloxacin, respectively.

WO_3 was chosen as the basis for the EEM to develop cheaper and more efficient EEMs. Our results indicate that the n(electrons)/n(WO_3) ratio is orders of magnitude larger than those previously reported in works that used POM ($[PW_{12}O_{40}]^{3-}$)[3] entrapped in silica sol−gel matrices. The synthesis process of EEMWO_3 is simple (it can also be easily commercialized), and because it can be reduced to its lower oxidation states, it is suitable for use as a reducing EEM besides entrapping an expensive active species that are not commercial, like EEMPOMs.[3] WO_3 is also known to be stable in acidic and oxidizing environments,[59] an important feature for catalytic degradation processes. The finding that tungsten oxide can function as an active EEM in the absence of entrapped redox species, therefore, is significant and can be exploited to markedly streamline the degradation process, in which the tungsten oxide plays a dual role both as a skeleton and as the redox species. This feature confers WO_3, a marked advantage that distinguishes it from other EEMs, in which a limited amount of active species can be entrapped in the matrix. In the case of WO_3, however, which plays a dual role in the EEM as both a matrix and also as a redox species, this may increase the electronic yield and, therefore, the efficiency of the treatment process.

Therefore, for such efficient EEMs a pure material that has a stable reduced or oxidized oxidation state and can be synthesized with a large surface area is needed. WO_3 is known to have a blue-reduced stable oxidation state.[60] Also, it is known that a sol−gel matrix features can be easily controlled according to the needs;[48] therefore, the sol−gel process was chosen for the EEEWO_3 synthesis (the process involves the hydrolysis and condensation of metal alkoxide precursors to produce a porous matrix,[7,31,61,62] which forms porous matrices with a large surface area.[48,62] In principle, one also could use for the reduction is MoO_3 particles, but its reduced form is a weaker reducing agent than the reduced form of WO_3. Therefore, we have chosen WO_3 for this study. The matrix was then reduced with $NaBH_4$ to obtain the reduced form of the matrix, after which the substrate, 4-nitrophenol (PNP) or 2-nitrophenol (ONP), was added to the system. Nitrophenols were chosen because they are common toxins in waste (0.002 mg/L of PNP in drinking water causes severe health problems; because of their toxicity, nitrophenols have been listed as among the worst industrial pollutants by the US Environmental Protection Agency).[43−46] Moreover, their stable structure renders them difficult to degrade, even at low concentrations. According to a report by the National Bureau of Statistics, 5432.25 tons per 70 billion tons of industrial wastewater in China have been polluted by phenol compounds, among which nitrophenols are included.[43] Therefore, the development of different methods to treat them in industrial settings, before they reach water sources, is important.[63−65] Most such methods in use today rely on heterogeneous catalysts, whose synthesis is complex. The use of the easily synthesized WO_3 as an EEM, therefore, could streamline the process. The results of this study indicate that certain features of the WO_3, especially its structure, affect the PNP and the ONP degradation processes.

The main objective of the current study was to apply, in practice, green engineering principles and to exploit the unique features of EEMWO_3 to develop an efficient, cheap, and simple treatment technique for toxic compounds, such as nitrophenols, that meets the standards of green engineering. The study's outcomes can contribute to the green engineering field, especially in the treatment of toxic compounds, as our initial results with nitrophenols indicate. Moreover, our treatment method can be applied to treat toxic industrial wastewater before it leaves the factory.

2. EXPERIMENTAL SECTION

2.1. Materials. Analytical grade reagents were purchased from Sigma-Aldrich: nitric acid, sodium tungstate dihydrate, citric acid mono hydrate, sodium phosphate, anhydrous sodium phosphate dibasic, hydrochloric acid, sodium hydroxide, 4-nitrophenol (PNP), 4-aminophenol (PAP), 2-nitrophenol (ONP), 2-aminophenol (OAP), sodium borohydride, acetonitrile, formic acid. Argon was purchased from Maxima. Commercial WO_3 was purchased from Apollo Scientific.

All solutions were prepared using deionized water that was purified by filtering it through a Milli-Q Millipore setup with a final resistivity >10 MΩ·cm.

2.2. Stages of the Study. (1) WO_3 particles (symbolized: EEMWO_3) were synthesized according to a sol−gel procedure[66] (Figure 1a). The full description of the synthesis is in Section S1. (2) 2.16×10^{-3} mol EEMWO_3 was mixed with water under Ar atmosphere for 10 min (at pH 3 or 10, Figure 1b). (3) 7.93×10^{-4} mol $NaBH_4$ was then added to the mixture to obtain the reduced form of the matrix during mixing. The $NaBH_4$/EEEMWO_3 ratio equals 0.37, and considering the number of the electrons which $NaHB_4$ could give, it equals 2.9 (($NaBH_4$/EEEMWO_3)X8). Therefore, there is an excess of reductive material. Next, the vile was surrounded by ice (in order to decrease the rate of the water reduction) and deaerated with Ar for 2 h, during which the color of the matrix changed from yellow to blue (Figure 1c). (4) The reduced matrices were mixed for 24 h with PNP (7.19×10^{-5} mol) or ONP (7.19×10^{-5} mol) solution (at room temperature), and the color of the mixture changed again from blue to yellow (Figure 1d). (5) Lastly, the matrices were separated from the reaction solutions by filtration, and the filtrates were injected into a high-performance liquid chromatograph (HPLC). The experiments were done with WO_3, which was synthesized EEMWO_3, and with a commercial WO_3 (symbolized: EEMWO_3-Com). The degradation process was done in a close vile that was not opened between the stages but only between the cycles.

The synthesized and the commercial EEMWO_3 particles were characterized before and after the process by scanning electron microscopy (SEM), X-ray diffractometry (XRD), X-ray photoelectron spectroscopy (XPS), and Brunauer−Emmett−Teller (BET) analysis.

https://doi.org/10.1021/acsomega.4c08455
ACS Omega 2025, 10, 10878−10890

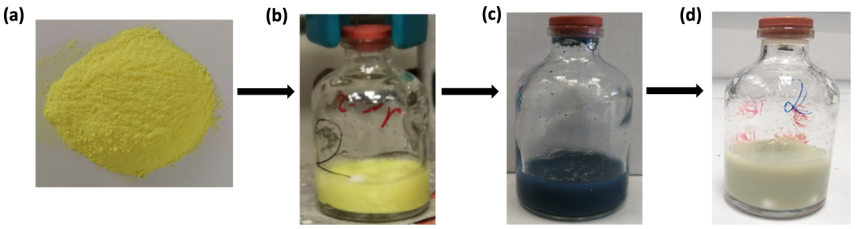

Figure 1. (a) $EEMWO_3$ powder, (b) 1.08×10^{-3} mol $EEMWO_3$ with water, (c) 1.08×10^{-3} mol $EEMWO_3$ after addition of 2.64×10^{-4} mol $NaBH_4$, (d) 1.08×10^{-3} mol $EEMWO_3$ after addition of 2.64×10^{-4} mol $NaBH_4$ and mixing 24 h with 7.19×10^{-6} mol PNP at pH 3. Photograph courtesy of Lior Carmel.

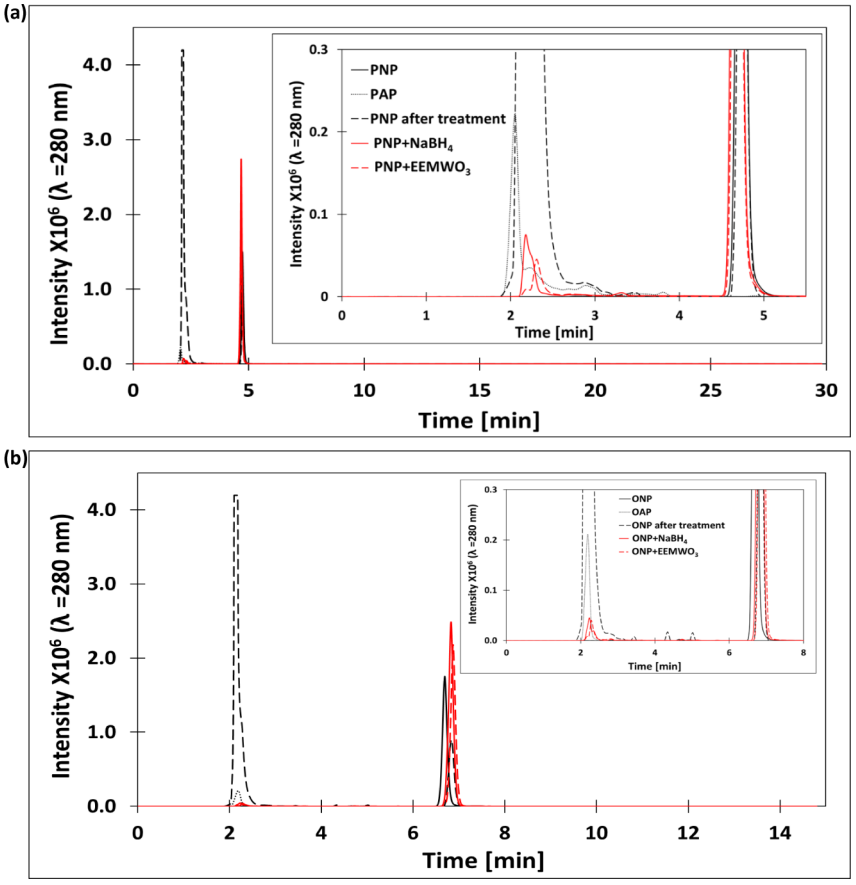

Figure 2. Chromatographs of solutions before and after treatment. (a) 1.0×10^{-4} M PNP, 4.0×10^{-4} M PAP, PNP at pH 3 after treatment. The treatment included mixing 2.64×10^{-4} mol $NaBH_4$ with 1.08×10^{-3} mol $EEMWO_3$ and 1.0×10^{-4} M PNP at pH 3. (b) 9.0×10^{-5} M ONP, 9.0×10^{-5} M OAP, ONP after treatment, which included mixing 2.64×10^{-4} mol $NaBH_4$ with 1.08×10^{-3} mol $EEMWO_3$ and 9.0×10^{-5} M ONP at pH 3.

2.3. Scanning Electron Microscopy (SEM). SEM FEI, Thermo Fisher Scientific (various 460L, 161 Hillsboro, Oregon, United States), and energy-dispersive X-ray spectroscopy (EDS) X-MaxN 80 (Oxford Instruments, Oxford, Britain) instruments were used to characterize the morphological surfaces of $EEMWO_3$ before and after its reactions with $NaBH_4$ and after its reaction with substrate.

2.4. X-Ray Diffractometry (XRD). Samples were characterized by the X-ray powder diffraction method by using a Panalytical Empyrean II multipurpose diffractometer (Panalytical B.V., Almelo, The Netherlands) equipped with a position sensitive X'Celerator detector. Data were collected in Bragg–Brentano ($\theta/2\theta$) geometry using a Cu K_α radiation (λ = 1.54178 Å) source at 40 kV and 30 mA. Crystallographic structural and phase identification analysis of WO_3 and related hydrated phases was performed using the Match! crystallographic analysis software (version 2.1.1) and coupled with the International Center for Diffraction Data (ICDD) Powder Diffraction File (PDF-4+) database (2022). The PowderCell program suite (version 2.4) was then used to perform Rietveld structure refinement and to produce unit cell diagrams. The synthesized and the commercial WO_3 were characterized, and their structures were shown to fit those published in the literature.[67,68]

2.5. X-Ray Photoelectron Spectroscopy (XPS). An X-ray photoelectron spectrometer ESCALAB -Xi$^+$ ultrahigh vacuum (1×10^{-9} bar) apparatus with an Al K^α X-ray source and a monochromator was used to collect XPS data. The X-ray beam size was 500 μm, and survey spectra were recorded with a pass energy (PE) of 150 eV, and high energy resolution

https://doi.org/10.1021/acsomega.4c08455
ACS Omega 2025, 10, 10878−10890

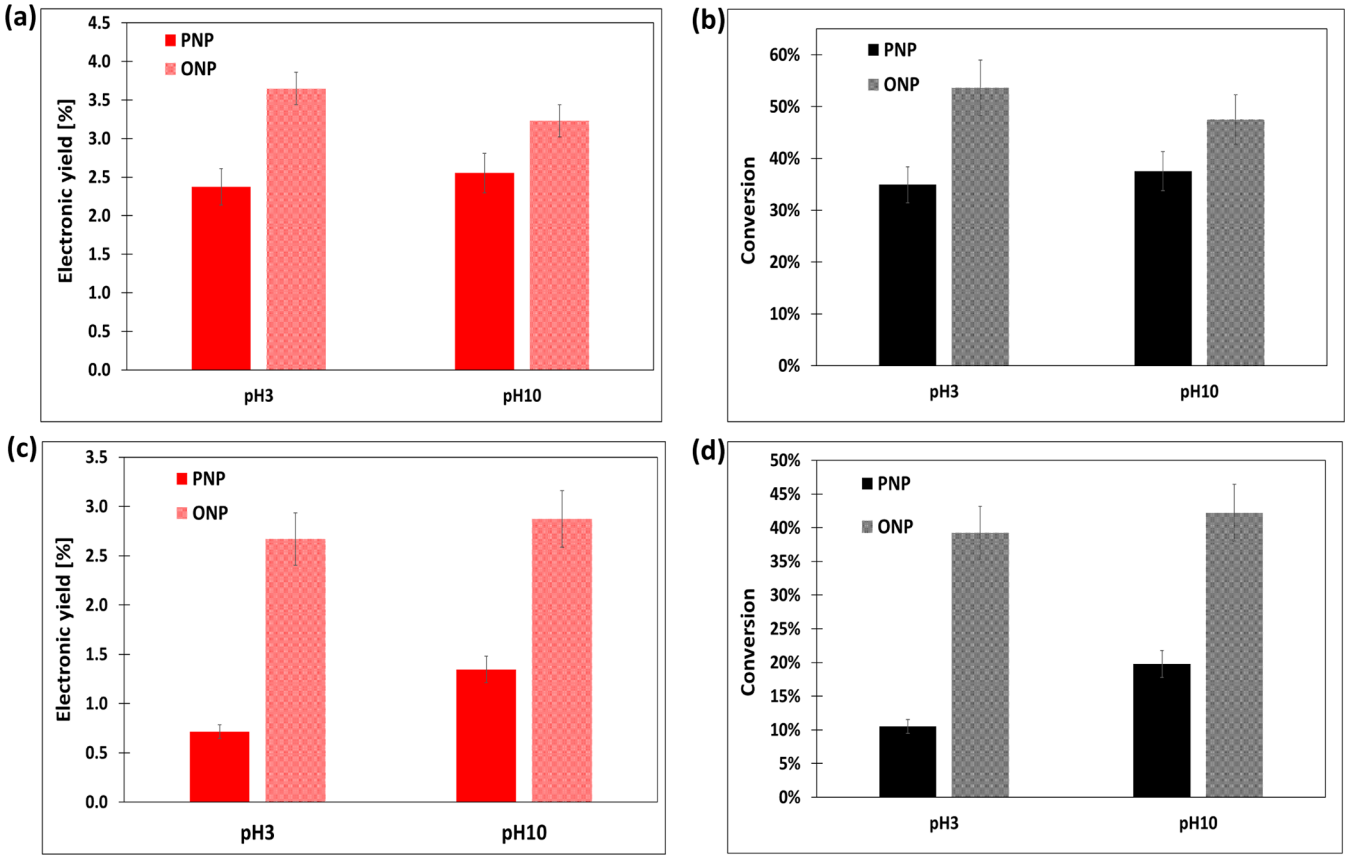

Figure 3. Conversion, % decrease of PNP/ONP concentration, and electronic yield of PNP and ONP. (a) and (b) 2.16×10^{-3} mol $EEMWO_3$ was mixed for 2 h with 7.93×10^{-4} mol $NaBH_4$ (($NaBH_4$/$EEMWO_3$)X8 = 2.9) and then mixed for 24 h with 7.19×10^{-5} mol PNP/ONP at pH 3 or 10. (c) and (d) 2.16×10^{-3} mol $EEMWO_3$-Com was mixed for 2 h with 7.93×10^{-4} mol $NaBH_4$ (($NaBH_4$/$EEMWO_3$)X8 = 2.9) and then mixed for 24 h with 7.19×10^{-5} mol PNP/ONP at pH 3 and 10.

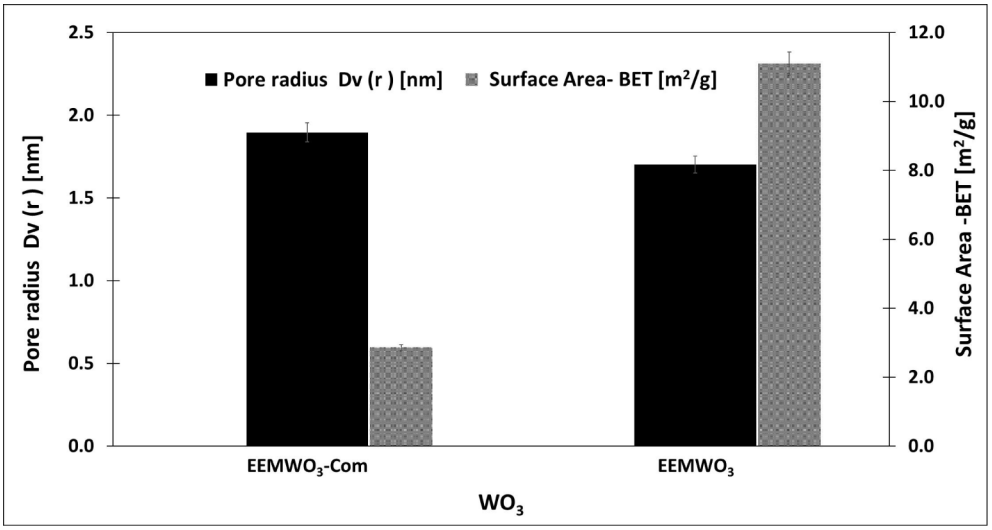

Figure 4. BET measurements of $EEMWO_3$ and $EEMWO_3$-Com.

spectra were recorded with a PE of 20 eV. To correct for charging effects, all spectra were calibrated relative to a carbon C 1s peak positioned at 284.8 eV. The atomic ratios were calculated from the peak intensity ratios and the reported atomic sensitivity factors.

2.6. BET (Brunauer–Emmett–Teller) Analysis. The tested matrices underwent surface area analyses by using a Quantachrome NOVAtouch LX3 surface analyzer (N_2 at 77 K). The measurements were carried out using nitrogen gas (99.999% pure, from Maxima), and the specific surface areas were calculated according to the BET curve.

2.7. High Performance Liquid Chromatography (HPLC). The reactants and the products concentration were measured by HPLC (Jasco XLC-3059AS) with a C18 4E column. The mobile phase contains 50% acetonitrile, 50% deionized water and 0.1% formic acid. The HPLC injection

https://doi.org/10.1021/acsomega.4c08455
ACS Omega 2025, 10, 10878−10890

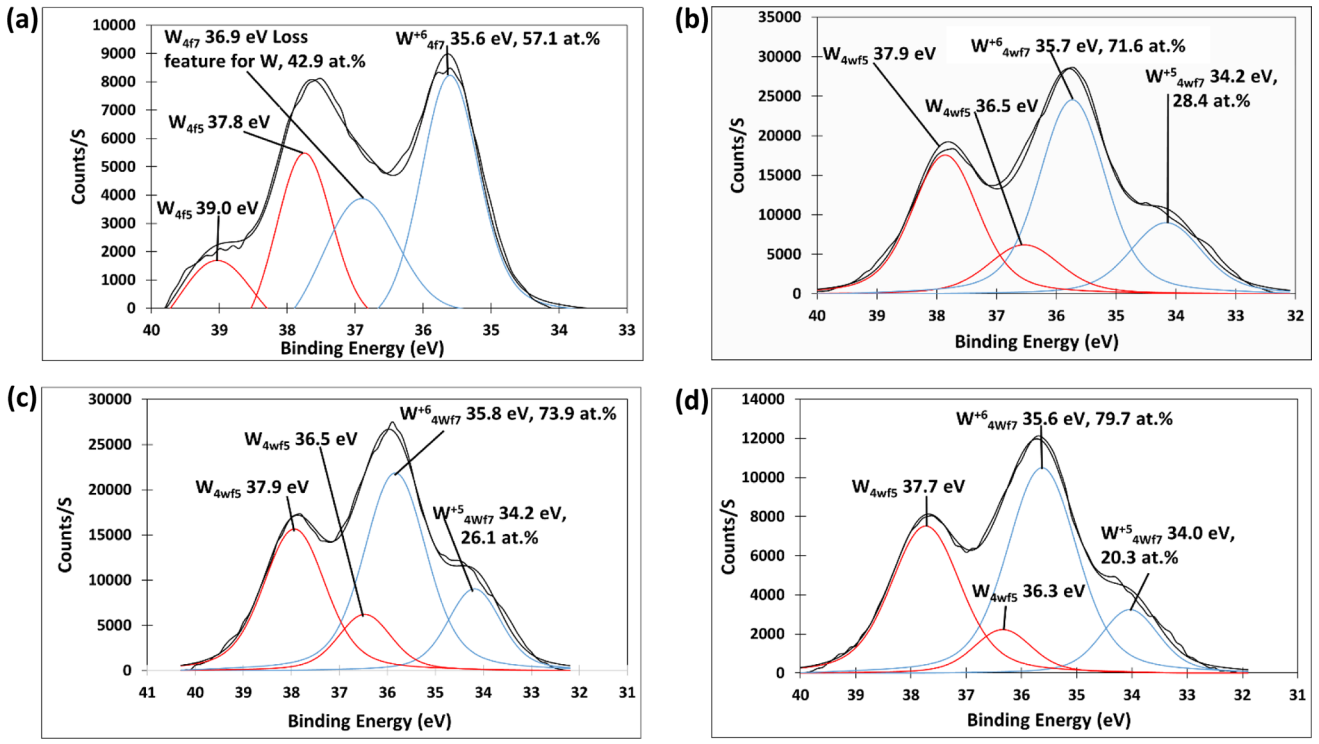

Figure 5. XPS results − the experiments were done with 1.08×10^{-3} mol $EEMWO_3$, 2.64×10^{-4} mol $NaBH_4$, 1.80×10^{-6} mol PNP/ONP at pH 3. (a) $EEMWO_3$, (b) $EEMncWO_3$ after $NaBH_4$ addition, (c) $EEMWO_3$ after $NaBH_4$ and PNP addition, (d) $EEMWO_3$ after $NaBH_4$ and ONP addition. It is important to note that each XPS measurement is a different $EEMWO_3$ sample (the sample was not measured from the beginning of the process to the end with the same dose of $EEMWO_3$). The energy values of the peaks fit those that are reported in the literature.[77,78]

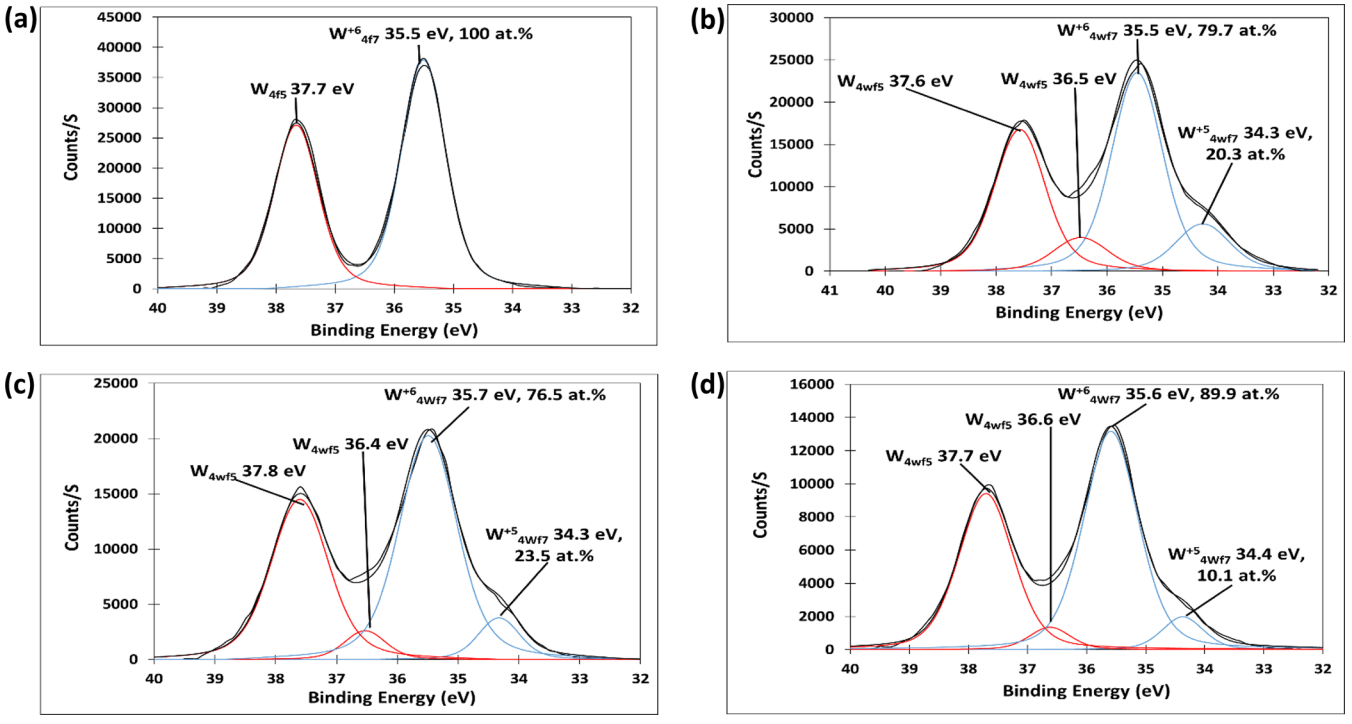

Figure 6. XPS results−the experiments were done with 1.08×10^{-3} mol $EEMWO_3$-Com, 2.64×10^{-4} mol $NaBH_4$, 1.80×10^{-6} mol PNP/ONP at pH 3. (a) $EEMWO_3$-Com, (b) $EEMWO_3$-Com after $NaBH_4$ addition, (c) $EEMWO_3$-Com after $NaBH_4$ and PNP addition, (d) $EEMWO_3$-Com after $NaBH_4$ and ONP addition. The energy values of the peaks fit those that are reported in the literature.[77,78]

conditions were 40 μL sample volume and a flow rate of 1 mL/min. The HPLC measurements were done at 280 nm, which was determined by the spectra of PNP, PAP, ONP, and OAP (Figure S1).

https://doi.org/10.1021/acsomega.4c08455
ACS Omega 2025, 10, 10878−10890

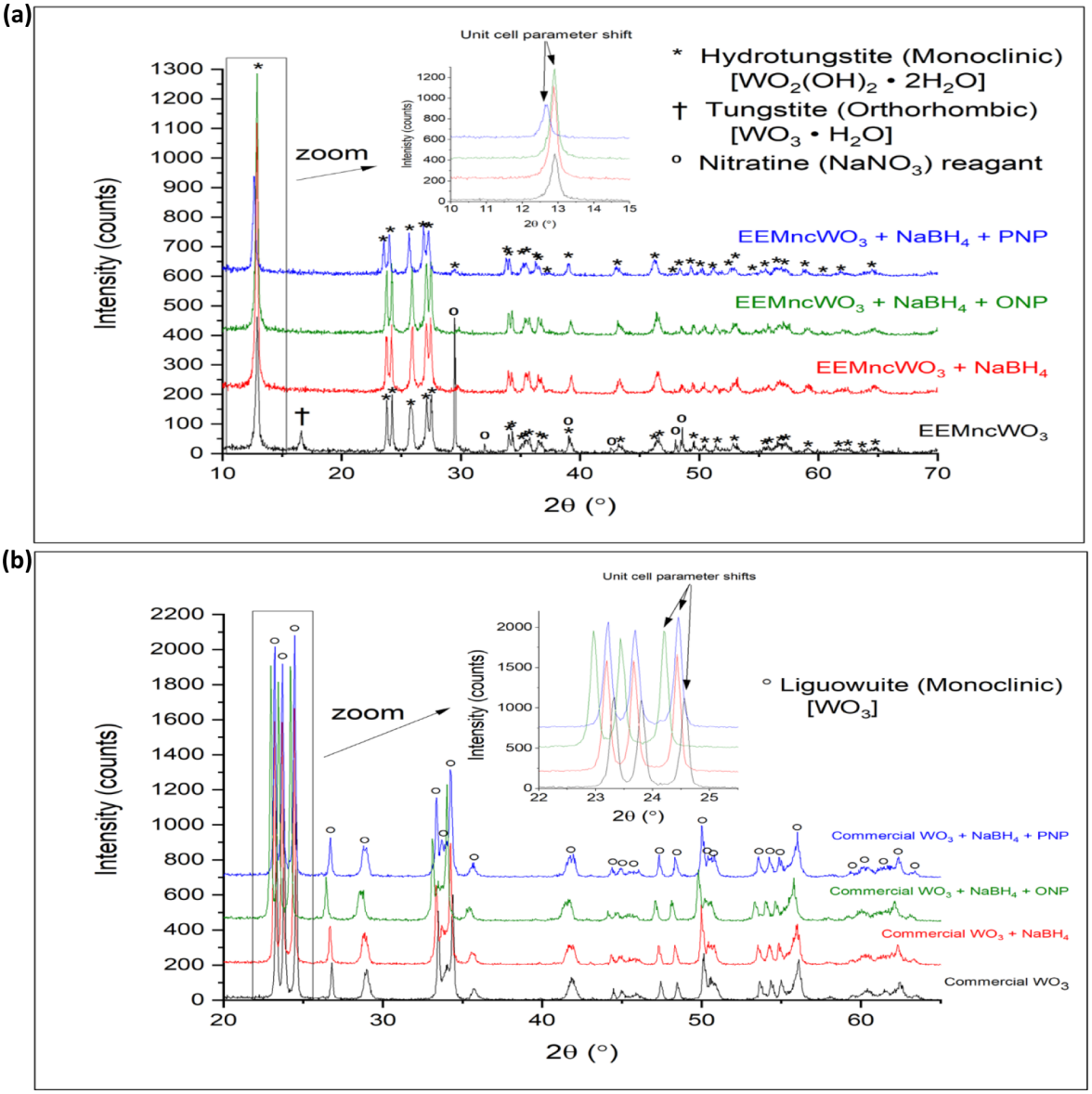

Figure 7. XRD of the EEM materials before and after the addition of the selected toxins (substrates). (a) Phase changes of the synthesized $EEMWO_3$. (b) Phase changes of the $EEMWO_3$-Com. The experiments were done with 1.08×10^{-3} mol $EEMWO_3$/$EEMWO_3$-Com, 2.64×10^{-4} mol $NaBH_4$, 1.80×10^{-6} mol PNP/ONP at pH 3.

3. RESULTS AND DISCUSSION

Two common toxic compounds that are soluble in water were chosen to develop an EEM for a toxin degradation process: p-nitrophenol (PNP) and o-nitrophenol (ONP). After mixing the reagents as described in the Materials and Methods section, the mixture was filtered at the end of the degradation process, and the filtrate was injected into the HPLC. The results show that after the degradation process, the amount of PNP/ONP decreased, and product peaks appeared (Figure 2). Control experiments indicated that neither PNP nor ONP reacted with either WO_3 or BH_4^-, as each is alone in the solution (Figure 2). According to previously published work[69,70] and the HPLC result of this study, the products for PNP degradation were 4-aminophenol (PAP) and acetaminophen, while for ONP degradation, the product was 2-aminophenol (OAP).

The conversion and electronic yield of the degradation processes of PNP and ONP at the two pH values that were studied (pH 3 and 10) are similar (Figure 3). The conversion and the electronic yield are defined in Section S2. Photoactivation and electrochemistry methods are common ways to achieve WO_3 activation.[71] In the current study, the reduction of $EEMWO_3$ was done by $NaBH_4$. WO_3 is a known catalyst for water reduction by $NaBH_4$,[60] which could be a parallel and competitive reaction with PNP/ONP reduction.

The occurrence of this parallel but competitive reaction may at least partially explain the obtained conversion results of around 10−50%, depending on the $EEMWO_3$ type (synthesized/commercial) and the substrate (PNP/ONP). The conversion values of catalytic processes reported in the literature are higher,[43,72−75] Table S1. It is important to note that the present study is focused on EEM, and the published studies are catalytic systems. Also, each EEM's capacity depends on the amount of material used to build the EEM, Figure S2.

https://doi.org/10.1021/acsomega.4c08455
ACS Omega 2025, 10, 10878−10890

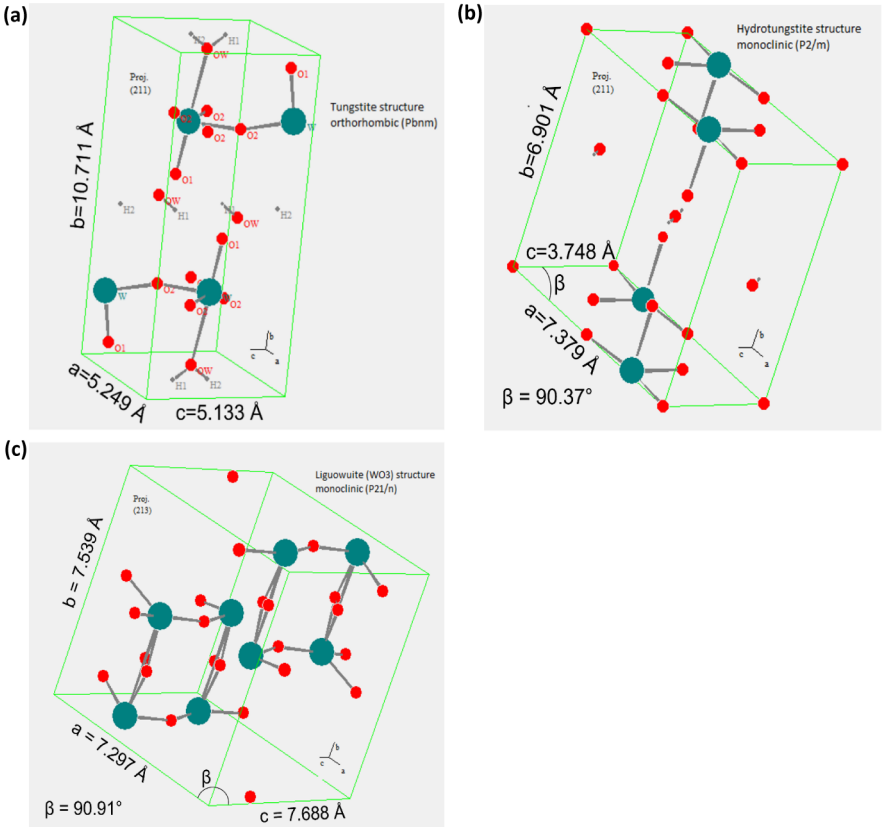

Figure 8. Unit-cell diagrams of the identified W-oxide structures found in the tungsten catalyst samples before and after the degradation process. (a) orthorhombic tungstite ($WO_3{\cdot}H_2O$), (b) monoclinic hydrotungstite ($WO_2(OH)_2{\cdot}H_2O$), (c) monoclinic liguowuite (WO_3).

However, the results indicate that this system enables a much larger ratio of electrons per mole WO_3 (the ratio is defined in Section S2 of) compared to that in EEMPOM systems, i.e., 0.1 and (0.0005−0.003) for $EEMWO_3$ and EEMPOM, respectively. This value was calculated without the assumption that the reaction occurs only on the surface of the $EEMWO_3$, which is assumed to be the case, and as such, not all of the tungsten participates in the process. Thus, the electrons per mole WO_3 ratio, an important parameter in degradation processes that occur during redox processes, is relatively high.

The degradation of PNP was expected to be higher[76] because of the steric hindrance in ONP, but that was not the case. The higher degradation observed instead for ONP may be due to the less positive electronic density of the ONP nitrogen, thus rendering it more attractive to the WO_3 for electron transfer and causing it to bind more strongly to the WO_3 surface.

Although the synthesis of $EEMWO_3$ is simple,[66] a $EEMWO_3$−Com reagent was also studied as a potential $EEMWO_3$ for comparison. The results of the comparison show that the conversion with the synthesized $EEMWO_3$ was larger than that with $EEMWO_3$−Com.

Recent results indicate that the conversion process may be affected by the structure of WO_3 in a manner similar to that observed in recent work, wherein the hydrated WO_3 exhibited more efficiency than its nonhydrated form as a catalyst in water reduction.[60] SEM, XPS, and XRD analyses were therefore done before and after the $EEMWO_3$ and $EEMWO_3$-Com were mixed with $NaBH_4$ and PNP/ONP.

BET analysis results indicate that the average surface area of $EEMWO_3$-Com particles was smaller than that of the synthesized $EEMWO_3$ particles (Figure 4), which could explain the lower conversion obtained for the former.

XPS measurements that analyze only the sample's surface indicate that most of the $EEMWO_3$ was not reduced (maximum ∼30% was reduced) (Figures 5 and 6). This means that only part of the tungsten present on the $EEMWO_3$ surface was reduced. The surface area of the synthesized $EEMWO_3$ was larger than that of the commercial variety (Figure 4), a finding that explains the higher conversion obtained with the synthesized $EEMWO_3$.

According to published results,[60] the structure of $EEMWO_3$ may affect process efficiency. Therefore, XRD measurements were done to analyze the structural differences between the WO_3-based EEMs (Figures 7 and 8). After the reaction with synthesized $EEMWO_3$, the dominant phase was monoclinic hydrotungstite ($WO_2(OH)_2{\cdot}H_2O$, Figure 8b), while the orthorhombic tungstite ($WO_3{\cdot}H_2O$, Figure 8a) reacted and could not be detected in the sample by XRD (Figure 7a). The monoclinic hydrotungstite present in the synthesized $EEMWO_3$ material continued to react, which was evident due to the changes in unit cell parameters and the broadening of the XRD peaks (Figure 7, inset). In contrast, both before and after the reaction with $EEMWO_3$-Com, the dominant phase was still the unhydrated, monoclinic liguowuite (WO_3, Figure 8c), which exhibited small unit cell parameter shifts that depended on the additional reagents present (Figure 7b, inset). The results obtained in this study are consistent with those presented in earlier works[60] in which the hydrated WO_3 phases were suggested to be more reactive and more efficient catalysts than the nonhydrated WO_3 phases. Similarly, the hydrated synthesized $EEMWO_3$ materials were more reactive, which led

https://doi.org/10.1021/acsomega.4c08455
ACS Omega 2025, 10, 10878−10890

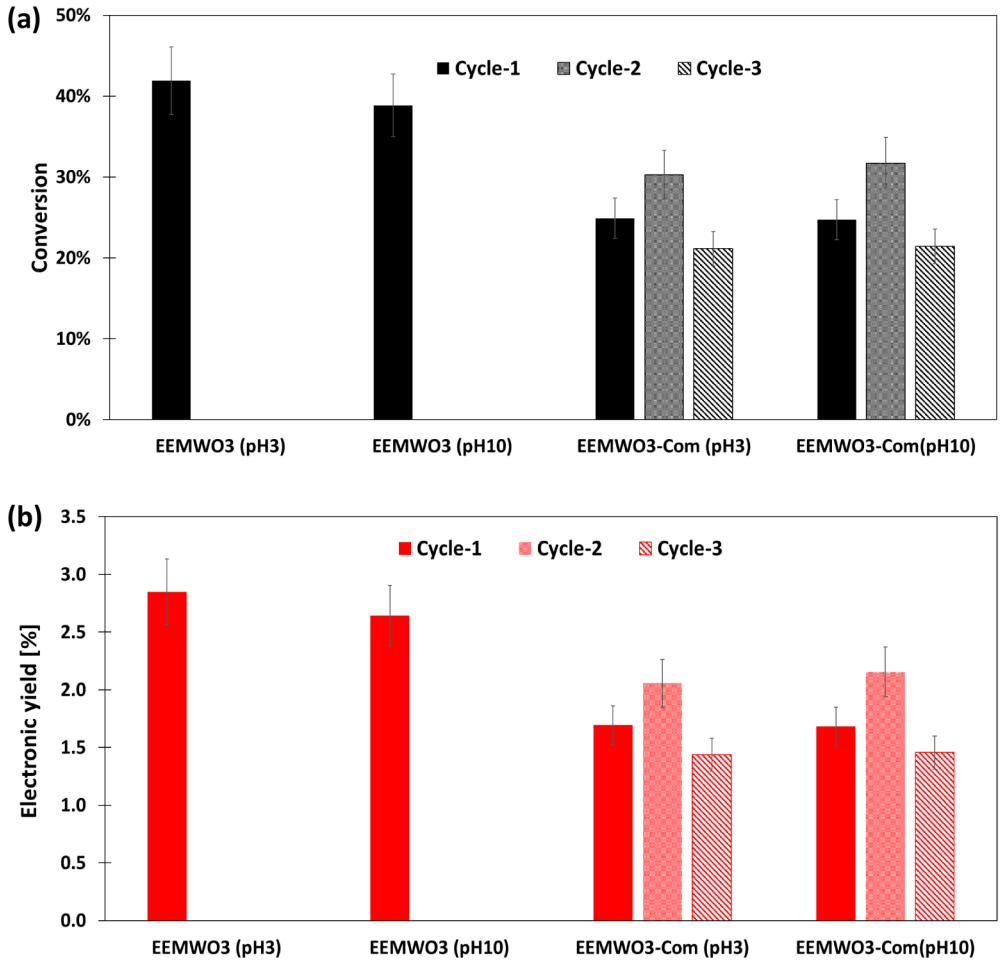

Figure 9. (a) Conversion, percentage decrease in PNP concentration, and (b) electronic yield of PNP − 2.16×10^{-3} mol $EEMWO_3$ was mixed for 2 h with 7.93×10^{-4} mol $NaBH_4$ and then mixed for 24 h with 7.19×10^{-5} mol PNP at pH 3 and 10.

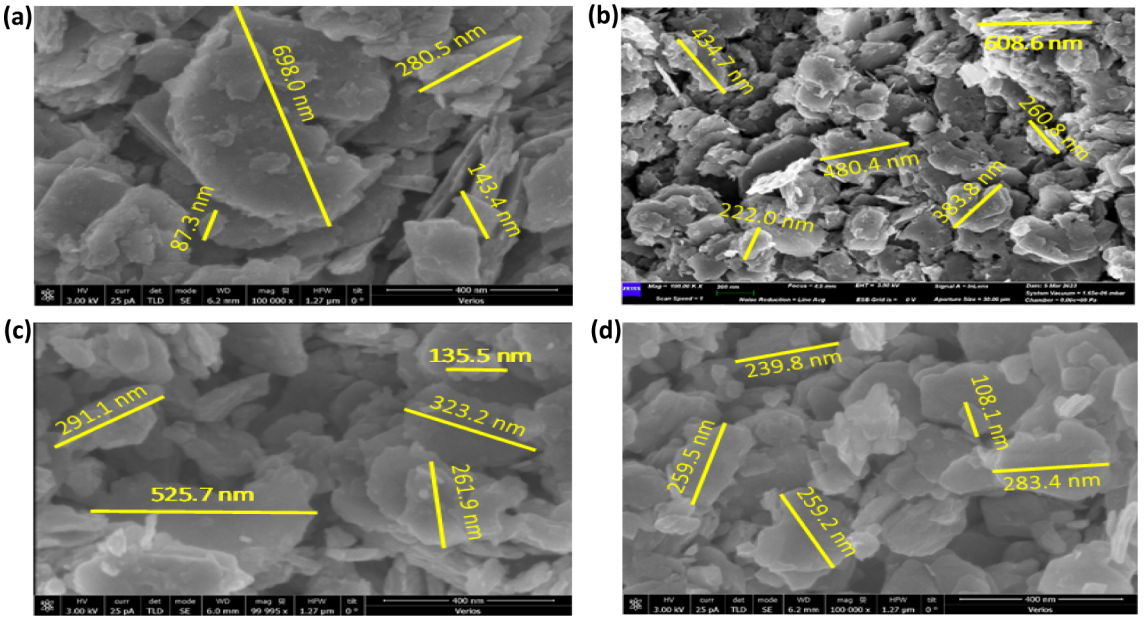

Figure 10. SEM images − the experiments were done with 1.08×10^{-3} mol $EEMWO_3$, 2.64×10^{-4} mol $NaBH_4$, 8.00×10^{-6} mol PNP/7.19×10^{-6} mol ONP. (a) $EEMWO_3$, (b) $EEMncWO_3$ after $NaBH_4$ addition, (c) $EEMWO_3$ after $NaBH_4$ and ONP addition, (d) $EEMWO_3$ after $NaBH_4$ and PNP addition.

https://doi.org/10.1021/acsomega.4c08455
ACS Omega 2025, 10, 10878−10890

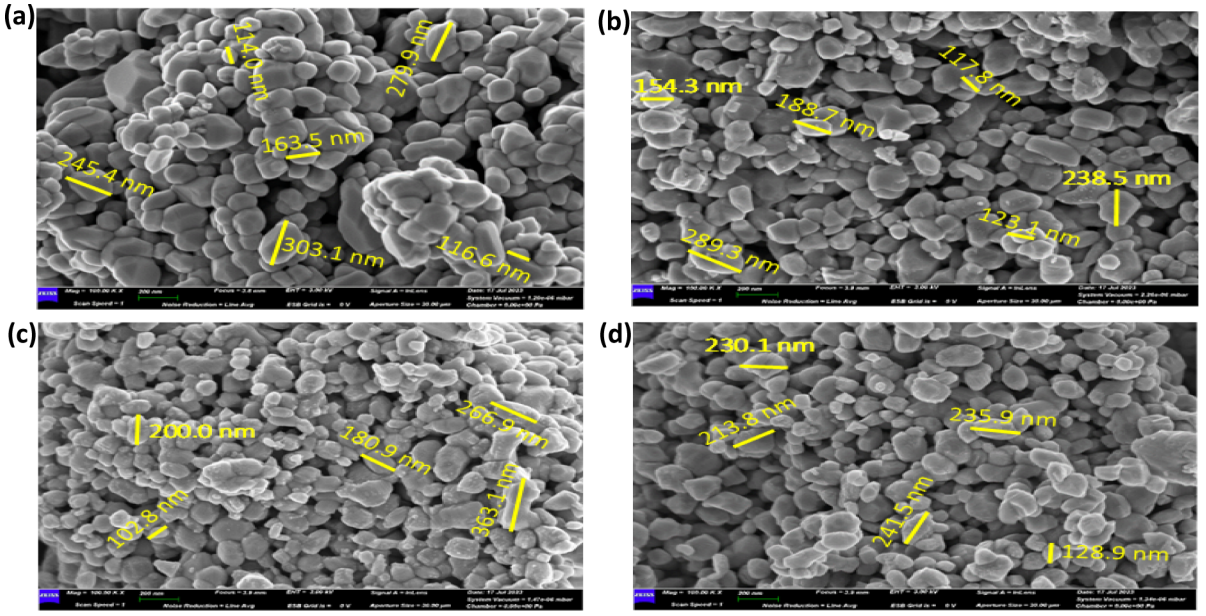

Figure 11. SEM images − the experiments were done with 1.08×10^{-3} mol EEMWO$_3$-Com, 2.64×10^{-4} mol NaBH$_4$, 8.00×10^{-6} mol PNP/7.19×10^{-6} mol ONP. (a) EEMWO$_3$-Com, (b) EEMncWO$_3$ after NaBH$_4$ addition, (c) EEMWO$_3$-Com after NaBH$_4$ and ONP addition, (d) EEMWO$_3$-Com after NaBH$_4$ and PNP addition.

to higher conversion rates than those observed for the unhydrated EEMWO$_3$-Com material. The synthesized EEMWO$_3$ also had more structural variability, and its tungstite (orthorhombic) phase was fully converted to hydrotungstite (monoclinic). Some conversions also happen with the EEMWO$_3$-Com material. The unit cell parameter shifts suggested by the small changes to the locations of major diffraction peaks with different reagents imply that slight structural changes occurred as a result of the reaction with the added PNP and ONP. Those results indicate that the conversion depends on the structure of the active species.

Independent of the type of EEMWO$_3$ used, the pH decreased after water was added to the EEMWO$_3$ during stage 2 (Figure 1 and Table S2; see Materials and Methods for a complete description of the stages of the experiment). This result is attributed to the zero point of charge of the W−OH groups on the surfaces of the EEMWO$_3$, which was ~4,[79] i.e., it is a weak acid.

After the addition of NaBH$_4$ (stage 3 Figure 1), reactions 1 and 2 occurred, and blue tungsten was formed.[60] This step depends on the surface area of the EEMWO$_3$; therefore, not all of the tungsten was reduced.

$$BH_4^- + 3H_2O + H^+ \rightarrow B(OH)_3/BO_2^- + 4H_2 \quad (1)$$

$$BH_4^- + WO_3 + nH_2O \rightarrow \text{blue tungsten} + B(OH)_3/BO_2^- + 2H_2 \quad (2)$$

The final pH increased due to the pK_a of B(OH)$_3$[80] and to the C$_6$H$_4$(OH)(NH$_3^+$)[81] that formed. The additions of PNP and ONP lead to the formations of PAP and OAP, respectively, which are amines whose pK_a values are in the range of 4−5.5,[81] and therefore, the pH increased (stage 4, Figure 1 and Table S2). The blue tungsten reacted via reactions 3 and 4 with PNP and ONP, respectively.

It is possible that nitrophenols are adsorbed on the matrix, but as the blue color disappears and aminophenol is formed, a clear redox process occurs. At pH 3 the product, aminophenol,

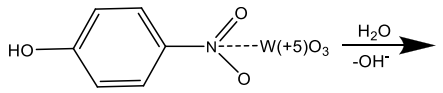

(3)

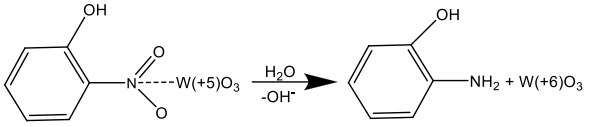

(4)

is a positively charged amine that will not adsorb to the matrix. The conversions at the two working pHs are similar, Figure 3, so also, at pH 10, the formation of the aminophenol does not hinder the redox process.

The key advantage of heterogeneous EEMs is their recyclability; therefore, cycle experiments were conducted to assess EEM reusability (Figure 9). In the first cycle, the synthesized EEMWO$_3$ had a larger conversion than the EEMWO$_3$-Com, but that tendency was reversed after the first cycle, and no PNP degradation occurred in the presence of the synthesized EEMWO$_3$. Each cycle led to reductions in the amount of synthesized EEMWO$_3$ because some of the material was lost during the washing between the cycles. This finding that material is lost could indicate that the structure of the synthesized EEMWO$_3$ was altered, thereby causing its dissolution. The conversion with the commercial EEM was not changed from cycle to cycle, indicating that its structure was more stable. According to the SEM measurements, the particles have a diameter of ca. hundreds of nanometers (Figures 10 and 11), and the sizes of the EEMWO$_3$ clusters in both the synthesized and the commercial EEMWO$_3$ were not changed during the first cycle.

https://doi.org/10.1021/acsomega.4c08455
ACS Omega 2025, 10, 10878−10890

4. CONCLUSIONS

The results show that the structure and the surface area of the EEMWO$_3$ are important parameters in the degradation processes of PNP and ONP, toxic organic compounds that are difficult to treat. The hydrated WO$_3$ phase is suggested to be a more reactive and more efficient catalyst than the nonhydrated WO$_3$ phase. In the current study, tungsten oxide had a dual role and functioned both as an active EEM with no entrapped redox species and as the skeleton. This dual functionality may confer on the EEMWO$_3$ a significant advantage in pollutant treatment processes, especially because it uses minimal amounts of chemicals, thus supporting the principles of green engineering. In addition, there is no limit to the amount of active species that can be entrapped in the matrix, which optimizes the process and increases the redox capacity. These advantages notwithstanding, the synthesized EEMWO$_3$ particles dissolve in the solution and cannot be recycled, and the redox process with the developed EEM occurs only on its surface. Future work with the EEMWO$_3$, therefore, should focus on increasing the device's surface area and its porosity.

Further studies are also needed to scale up the electron exchange columns to the industrial or semi-industrial level. The scaling-up stage of this process, however, is expected to entail several challenges, including the reproducibility of synthesizing the EEMWO$_3$ on a large scale, the effects on the reaction kinetics of performing large-scale reactions in larger reaction volumes, and the reduction with NaBH$_4$, which is an exothermic process accompanied by the evolution of hydrogen. In addition, the scale-up will involve the development of larger WO$_3$ particles and a more porous EEMWO$_3$ matrix. Insofar as these and other thermodynamic issues will be considered during the scale up process, it should be done gradually.

This study's results indicate that the EEMWO$_3$ is an efficient, simple, and cheap method with which to treat nitrophenols, which are common toxic aromatic compounds that are ubiquitous in industrial wastewater. Moreover, the findings reported herein, which show that fewer of the typically used solvent chemicals are needed to use the EEMWO$_3$, could promote the development of better, greener treatment methods that can be used to reduce the toxic compounds in wastewater.[82] Therefore, these results have significant implications for the field of green engineering in general and for the treatment of pollutants in particular.

■ ASSOCIATED CONTENT

Supporting Information

The Supporting Information is available free of charge at https://pubs.acs.org/doi/10.1021/acsomega.4c08455.

The spectra of the reactants and the products, a pH table during the process, and equations (PDF)

■ AUTHOR INFORMATION

Corresponding Authors

Dror Shamir − *Nuclear Research Centre Negev, Beer-Sheva 84190, Israel*; Email: drorshamir@gmail.com

Ariela Burg − *Chemical Engineering Department, Sami Shamoon College of Engineering, Beer-Sheva 8410802, Israel*; orcid.org/0000-0002-1888-4225; Email: arielab@sce.ac.il

Authors

Lior Carmel − *Chemical Sciences Department, Ariel University, Ariel 40700, Israel; Nuclear Research Centre Negev, Beer-Sheva 84190, Israel*

Shiran Aharon − *Chemical Sciences Department, Ariel University, Ariel 40700, Israel; Chemical Engineering Department, Sami Shamoon College of Engineering, Beer-Sheva 8410802, Israel*

Dan Meyerstein − *Chemical Sciences Department, Ariel University, Ariel 40700, Israel; Chemistry Department, Ben-Gurion University of the Negev, Beer-Sheva 8410501, Israel*

Yael Albo − *Chemical Engineering Department, Ariel University, Ariel 40700, Israel*; orcid.org/0000-0002-9873-0161

Lonia Friedlander − *Ilse Katz Institute for Nano-scale Science and Technology, Ilse Katz Institute for Nano-Scale Science and Technology, Ben-Gurion University of the Negev, Beer-Sheva 8410501, Israel*

Complete contact information is available at: https://pubs.acs.org/10.1021/acsomega.4c08455

Author Contributions

L.C.: data curation, HPLC measurements, design experiments. S.A.: BET measurements. D.M.: writing, supervision. Y.A.: writing. L.F.: XRD measurements. D.S.: data curation, supervision. A.B.: methodology, writing, supervision.

Notes

The authors declare no competing financial interest.

■ ACKNOWLEDGMENTS

The authors thank Dr. Dani Shahar of BioAnalytics, Ltd, and the designer Edna Rolnick for the TOC design.

■ REFERENCES

(1) Cassidy, H. G. Electron Exchange-Polymers. I. *J. Am. Chem. Soc.* **1949**, *71* (2), 402−406.

(2) Lavi, Y.; Burg, A.; Maimon, E.; Meyerstein, D. Electron Exchange Columns through Entrapment of a Nickel Cyclam in a Sol−Gel Matrix. *Chem. - Eur. J.* **2011**, *17* (18), 5188−5192.

(3) Singh, N.; Albo, Y.; Shamir, D.; Subramanian, P.; Goobes, G. Polyoxometalates entrapped in sol−gel matrices for reducing electron exchange column applications. *J. Coord. Chem.* **2016**, *69* (23), 3449−3457.

(4) Neelam; Albo, Y.; Burg, A.; Shamir, D.; Meyerstein, D. Bromate reduction by an electron exchange column. *Chem. Eng. J.* **2017**, *330*, 419−422.

(5) Neelam; Meyerstein, D.; Burg, A.; Shamir, D.; Albo, Y. Polyoxometalates entrapped in sol-gel matrices as electron exchange columns and catalysts for the reductive de-halogenation of halo-organic acids in water. *J. Coord. Chem.* **2018**, *71* (19), 3180−3193.

(6) Abudayyeh, A. M.; Mahmoud, L. A. M.; Ting, V. P.; Nayak, S. Metal−Organic Frameworks (MOFs) and Their Composites for Oil/Water Separation. *ACS Omega* **2024**, *9*, 47374−47394.

(7) Peled, Y.; Shamir, D.; Marks, V.; Kornweitz, H.; Albo, Y.; Yakhin, E.; Meyerstein, D.; Burg, A. Sol-gel matrices for the separation of uranyl and other heavy metals. *J. Environ. Chem. Eng.* **2022**, *10* (4), 108142.

(8) Massoumılari, Ş.; Velioğlu, S. Can MXene be the Effective Nanomaterial Family for the Membrane and Adsorption Technologies to Reach a Sustainable Green World? *ACS Omega* **2023**, *8* (33), 29859−29909.

(9) Sharma, V. K.; Feng, M. Water depollution using metal-organic frameworks-catalyzed advanced oxidation processes: A review. *J. Hazard. Mater.* **2019**, *372*, 3−16.

(10) Ubhi, M. K.; Kaur, M.; Grewal, J. K.; Oliveira, A. C.; Garg, V. K.; Sharma, V. K. Insight into photocatalytic behavior of magnesium ferrite−bentonite nanocomposite for the degradation of organic contaminants. *J. Mater. Res.* **2023**, *38* (4), 990−1006.
(11) Sun, P.; Liu, H.; Feng, M.; Guo, L.; Zhai, Z.; Fang, Y.; Zhang, X.; Sharma, V. K. Nitrogen-sulfur co-doped industrial graphene as an efficient peroxymonosulfate activator: Singlet oxygen-dominated catalytic degradation of organic contaminants. *Appl. Catal., B* **2019**, *251*, 335−345.
(12) Neelam; Meyerstein, D.; Adhikary, J.; Burg, A.; Shamir, D.; Albo, Y. Zero-valent iron nanoparticles entrapped in SiO2 sol-gel matrices: A catalyst for the reduction of several pollutants. *Catal. Commun.* **2020**, *133*, 105819.
(13) Bresler, K.; Shamir, D.; Shamish, Z.; Meyerstein, D.; Burg, A. Detailed mechanism of organic pollutant oxidation via the heterogeneous Fenton reaction requires using at least two substrates, e.g.: DMSO and EtOH. *J. Environ. Chem. Eng.* **2023**, *11* (1), 109140.
(14) Kumari, M.; Pulimi, M. Sulfate Radical-Based Degradation of Organic Pollutants: A Review on Application of Metal-Organic Frameworks as Catalysts. *ACS Omega* **2023**, *8* (38), 34262−34280.
(15) Klančič, V.; Gobec, M.; Jakopin, Ž. Halogenated ingredients of household and personal care products as emerging endocrine disruptors. *Chemosphere* **2022**, *303*, 134824.
(16) Sharma, A.; Vázquez, L. A. B.; Hernández, E. O. M.; Becerril, M. Y. M.; Oza, G.; Ahmed, S. S. S. J.; Ramalingam, S.; Iqbal, H. M. N. Green remediation potential of immobilized oxidoreductases to treat halo-organic pollutants persist in wastewater and soil matrices - A way forward. *Chemosphere* **2022**, *290*, 133305.
(17) Zhang, M.; Shi, Q.; Song, X.; Wang, H.; Bian, Z. Recent electrochemical methods in electrochemical degradation of halogenated organics: A review. *Environ. Sci. Pollut. Res.* **2019**, *26* (11), 10457−10486.
(18) Yan, Z.; Ouyang, J.; Wu, B.; Liu, C.; Wang, H.; Wang, A.; Li, Z. Nonmetallic modified zero-valent iron for remediating halogenated organic compounds and heavy metals: A comprehensive review. *Environ. Sci. Ecotechnol.* **2024**, *21*, 100417.
(19) King, J. F.; Mitch, W. A. Electrochemical reduction of halogenated organic contaminants using carbon-based cathodes: A review. *Crit. Rev. Environ. Sci. Technol.* **2024**, *54* (4), 342−367.
(20) Shamir, D.; Elias, I.; Albo, Y.; Meyerstein, D.; Burg, A. ORMOSIL-entrapped copper complex as electrocatalyst for the heterogeneous de-chlorination of alkyl halides. *Inorg. Chim. Acta* **2020**, *500*, 119225.
(21) Meistelman, M.; Meyerstein, D.; Bardea, A.; Burg, A.; Shamir, D.; Albo, Y. Reductive Dechlorination of Chloroacetamides with NaBH4 Catalyzed by Zero Valent Iron, ZVI, Nanoparticles in ORMOSIL Matrices Prepared via the Sol-Gel Route. *Catalysts* **2020**, *10* (9), 986.
(22) Ahmaruzzaman, M.; Roy, P.; Bonilla-Petriciolet, A.; Badawi, M.; Ganachari, S. V.; Shetti, N. P.; Aminabhavi, T. M. Polymeric hydrogels-based materials for wastewater treatment. *Chemosphere* **2023**, *331*, 138743.
(23) Subhan, F.; Aslam, S.; Yan, Z.; Yaseen, M.; Khan, K. A. Palladium nanoparticles decorated on ZSM-5 derived micro-/mesostructures (MMZ) for nitrophenol reduction and MB degradation in water. *J. Environ. Chem. Eng.* **2021**, *9* (1), 105002.
(24) Elfiad, A.; Galli, F.; Boukhobza, L. M.; Djadoun, A.; Boffito, D. C. Low-cost synthesis of Cu/α-Fe2O3 from natural HFeO2: Application in 4-nitrophenol reduction. *J. Environ. Chem. Eng.* **2020**, *8* (5), 104214.
(25) Manjula, M. C.; Nagashree, K. L.; Manjunatha, S.; Kolathur Ramachandra, S.; Nanda, N.; Ramachandra, P. Solution combustion synthesis of Ag decorated CeO2 nanocomposite for the reduction of nitroaromatic compounds. *Inorg. Chem. Commun.* **2024**, *168*, 112858.
(26) Saikia, P.; Borah, D.; Debnath, R.; Gogoi, D.; Goswami, K. J.; Rout, J.; Ghosh, N. N.; Bhattacharjee, C. R. Green sustainable synthesis of Ag doped SnO2 decorated reduced graphene oxide hierarchical nanohybrid material: An excellent mesoporous catalyst for efficient reduction of nitroaromatics. *J. Environ. Chem. Eng.* **2024**, *12* (4), 113137.
(27) Kaur, M.; Nagaraja, C. M. Template-Free Synthesis of Zn1−xCdxS Nanocrystals with Tunable Band Structure for Efficient Water Splitting and Reduction of Nitroaromatics in Water. *ACS Sustainable Chem. Eng.* **2017**, *5* (5), 4293−4303.
(28) Krishna Kumar, A. S.; Lu, C.-Y.; Tseng, W.-L. Two in One: Poly(ethyleneimine)-Modified MnO2 Nanosheets for Ultrasensitive Detection and Catalytic Reduction of 2,4,6-Trinitrotoluene and Other Nitro Aromatics. *ACS Sustainable Chem. Eng.* **2021**, *9* (3), 1142−1151.
(29) Meistelman, M.; Meyerstein, D.; Burg, A.; Shamir, D.; Albo, Y. Doing More with Less": Ni(II)@ORMOSIL, a Novel Sol-Gel Pre-Catalyst for the Reduction of Nitrobenzene. *Catalysts* **2021**, *11* (11), 1391.
(30) Ansari, A.; Badhe, R. A.; Garje, S. S. Preparation of CdS−TiO2-Based Palladium Heterogeneous Nanocatalyst by Solvothermal Route and Its Catalytic Activity for Reduction of Nitroaromatic Compounds. *ACS Omega* **2019**, *4* (12), 14937−14946.
(31) Biton Seror, S.; Shamir, D.; Albo, Y.; Kornweitz, H.; Burg, A. Elucidation of a mechanism for the heterogeneous electro-fenton process and its application in the green treatment of azo dyes. *Chemosphere* **2022**, *286*, 131832.
(32) Innocenzi, V.; Prisciandaro, M.; Centofanti, M.; Vegliò, F. Comparison of performances of hydrodynamic cavitation in combined treatments based on hybrid induced advanced Fenton process for degradation of azo-dyes. *J. Environ. Chem. Eng.* **2019**, *7* (3), 103171.
(33) Meng, X.; Scheidemantle, B.; Li, M.; Wang, Y.-Y.; Zhao, X.; Toro-González, M.; Singh, P.; Pu, Y.; Wyman, C. E.; Ozcan, S.; Cai, C. M.; Ragauskas, A. J. Synthesis, Characterization, and Utilization of a Lignin-Based Adsorbent for Effective Removal of Azo Dye from Aqueous Solution. *ACS Omega* **2020**, *5* (6), 2865−2877.
(34) Ahlawat, K.; Jangra, R.; Prakash, R. Environmentally Friendly UV-C Excimer Light Source with Advanced Oxidation Process for Rapid Mineralization of Azo Dye in Wastewater. *ACS Omega* **2024**, *9* (13), 15615−15632.
(35) Jasmine, J.; Ponvel, K. M. Synthesis of Ag2CdS2/Carbon Nanocomposites for Effective Solar-Driven Dye Photodegradation and Electrochemical Application. *Es Energy Environ.* **2023**, *20*, 898.
(36) Kadam, P. A.; Jagtap, C. V.; Kadam, V. S.; Bhongale, C. J.; Prasad, B.; Gadave, K. M. Photodegradation of Methylene Blue Dye for Water Purification using Zinc Oxide (ZnO) Nanoparticles Synthesized by Acoustic Cavitation. *Es Energy Environ.* **2024**, *26*, 1230.
(37) Chen, H.; Lin, T.; Wang, P.; Zhang, X.; Jiang, F.; Liu, W. Treatment of bromate in UV/sulfite autoxidation process enhances formation of dibromoacetonitrile during chlorination. *Water Res.* **2022**, *225*, 119207.
(38) Adhikary, J.; Meyerstein, D.; Marks, V.; Meistelman, M.; Gershinsky, G.; Burg, A.; Shamir, D.; Kornweitz, H.; Albo, Y. Sol-gel entrapped Au0- and Ag0-nanoparticles catalyze reductive de-halogenation of halo-organic compounds by BH4−. *Appl. Catal., B* **2018**, *239*, 450−462.
(39) Singh, S.; Anil, A. G.; Kumar, V.; Kapoor, D.; Subramanian, S.; Singh, J.; Ramamurthy, P. C. Nitrates in the environment: A critical review of their distribution, sensing techniques, ecological effects and remediation. *Chemosphere* **2022**, *287*, 131996.
(40) Fajardo, A. S.; Westerhoff, P.; Sanchez-Sanchez, C. M.; Garcia-Segura, S. Earth-abundant elements a sustainable solution for electrocatalytic reduction of nitrate. *Appl. Catal., B* **2021**, *281*, 119465.
(41) Wang, Y.; Song, X.; Li, F. Thermal Behavior and Decomposition Mechanism of Ammonium Perchlorate and Ammonium Nitrate in the Presence of Nanometer Triaminoguanidine Nitrate. *ACS Omega* **2019**, *4* (1), 214−225.
(42) Dai, Y.-G.; Guo, X.-H.; Ma, G.-W.; Gai, W.-Z.; Deng, Z.-Y. Efficient Removal of Nitrate in Neutral Solution Using Zero-Valent Al Activated by Soaking. *ACS Omega* **2023**, *8* (28), 24922−24930.

https://doi.org/10.1021/acsomega.4c08455
ACS Omega 2025, 10, 10878−10890

(43) Zhang, J.; Chen, L.; Zhang, X. Removal of P-Nitrophenol by Nano Zero Valent Iron-Cobalt and Activated Persulfate Supported onto Activated Carbon. *Water* **2022**, *14* (9), 1387.
(44) Shokri, A. Degradation of 4-Nitrophenol from industrial wastewater by nano catalytic Ozonation. *Int. J. Nano Dimens.* **2016**, *7*, 160−167.
(45) Ma, Y.-S.; Huang, S.-T.; Lin, J.-G. Degradation of 4-nitrophenol using the Fenton process. *Water Sci. Technol.* **2000**, *42* (3−4), 155−160.
(46) Rambabu, D.; Pradeep, C. P.; Pooja; Dhir, A. Self-assembled material of palladium nanoparticles and a thiacalix[4]arene Cd(ii) complex as an efficient catalyst for nitro-phenol reduction. *New J. Chem.* **2015**, *39* (10), 8130−8135.
(47) Cohen, N.; Shamir, D.; Kornweitz, H.; Albo, Y.; Burg, A. Dual Role of Silicon-based Matrices in Electron Exchange Matrices for Waste Treatment. *ChemPhyschem* **2023**, *24* (18), No. e202300130.
(48) Burg, A.; Yadav, K. K.; Meyerstein, D.; Kornweitz, H.; Shamir, D.; Albo, Y. Effect of Sol−Gel Silica Matrices on the Chemical Properties of Adsorbed/Entrapped Compounds. *Gels* **2024**, *10* (7), 441.
(49) Song, J.; Huang, Z.-F.; Pan, L.; Zou, J.-J.; Zhang, X.; Wang, L. Oxygen-Deficient Tungsten Oxide as Versatile and Efficient Hydrogenation Catalyst. *ACS Catal.* **2015**, *5* (11), 6594−6599.
(50) Neumann, R.; Levin-Elad, M. Metal Oxide (TiO2, MoO3, WO3) Substituted Silicate Xerogels as Catalysts for the Oxidation of Hydrocarbons with Hydrogen Peroxide. *J. Catal.* **1997**, *166* (2), 206−217.
(51) Pyper, O.; Kaschner, A.; Thomsen, C. In situ Raman spectroscopy of the electrochemical reduction of WO3 thin films in various electrolytes. *Sol. Energy Mater. Sol. Cells* **2002**, *71* (4), 511−522.
(52) Can, F.; Courtois, X.; Duprez, D. Tungsten-Based Catalysts for Environmental Applications. *Catalysts* **2021**, *11* (6), 703.
(53) Mu, Z.; Liu, D.; Zhang, W.; Chai, D.; Dong, G.; Li, J.; Zhao, M. A Z-scheme heterojunction ZIF67/N, P-WO3 nanocomposite for photocatalytic degradation of levofloxacin. *J. Solid State Chem.* **2024**, *334*, 124660.
(54) Belousov, A. S.; Parkhacheva, A. A.; Shotina, V. A.; Titaev, D. N.; Suleimanov, E. V.; Shafiq, I. Engineering a staggered type-II Bi2WO6/WO3 heterojunction with improved photocatalytic activity in wastewater treatment. *Chemosphere* **2024**, *359*, 142316.
(55) Ga, S. J.; D, V. M.; S, R. A. K. Sago-shaped embedded Nanolayers of WO3/NiO/gC3N4 Nanohybrids for natural degradation of environmental pollutants: A photocatalytic sunlight mediated approach. *Chem. Phys. Impact* **2024**, *8*, 100571.
(56) Wang, L.; Liu, J.; Wang, Y.; Zhang, X.; Duan, D.; Fan, C.; Wang, Y. Insight into the enhanced photocatalytic performance of Ag3PO4 modified metastable hexagonal WO3. *Colloids Surf., A* **2018**, *541*, 145−153.
(57) Zhou, M.; Tian, X.; Yu, H.; Wang, Z.; Ren, C.; Zhou, L.; Lin, Y.-W.; Dou, L. WO3/Ag2CO3Mixed Photocatalyst with Enhanced Photocatalytic Activity for Organic Dye Degradation. *ACS Omega* **2021**, *6* (40), 26439−26453.
(58) Han, X.; Yao, B.; Li, K.; Zhu, W.; Zhang, X. Preparation and Photocatalytic Performances of WO_3/TiO_2 Composite Nanofibers. *J. Chem.* **2020**, *2020*, 2390486.
(59) Gondal, M.; Dastageer, M.; Khalil, A. Synthesis of nano-WO3 and its catalytic activity for enhanced antimicrobial process for water purification using laser induced photo-catalysis. *Catal. Commun.* **2009**, *11*, 214−219.
(60) Carmel, L.; Aharon, S.; Meyerstein, D.; Albo, Y.; Friedlander, L.; Shamir, D.; Burg, A. WO3 dehydration and phase transition as the catalytic driver of hydrogen production by non-calcinated WO3. *Int. J. Hydrogen Energy* **2024**, *51*, 1508−1520.
(61) Innocenzi, P. *Sol To Gel Transition*. SpringerCham: 2019.
(62) Aharon, S.; Meyerstein, D.; Tzur, E.; Shamir, D.; Albo, Y.; Burg, A. Advanced sol−gel process for efficient heterogeneous ring-closing metathesis. *Sci. Rep.* **2021**, *11* (1), 12506.
(63) Ji, Q.; Li, J.; Xiong, Z.; Lai, B. Enhanced reactivity of microscale Fe/Cu bimetallic particles (mFe/Cu) with persulfate (PS) for p-nitrophenol (PNP) removal in aqueous solution. *Chemosphere* **2017**, *172*, 10−20.
(64) Ma, A.; Yang, W.; Gao, K.; Tang, J.-Q. Concave Gold Nano-Arrows (Aucnas) for Efficient Catalytic Reduction of 4-Nitrophenol. *Chemosphere* **2023**, *310*, 136800.
(65) Truong, T. K.; Nguyen, T. Q.; Phuong La, H. P.; Le, H. V.; Van Man, T.; Cao, T. M.; Van Pham, V. Insight into the degradation of p-nitrophenol by visible-light-induced activation of peroxymonosulfate over Ag/ZnO heterojunction. *Chemosphere* **2021**, *268*, 129291.
(66) Chai, Y.; Ha, F. Y.; Yam, F. K.; Hassan, Z. Fabrication of Tungsten Oxide Nanostructure by Sol-Gel Method. *Procedia Chem.* **2016**, *19*, 113−118.
(67) Yoo, S.-J.; Kim, D.; Baek, S.-H. Controlled Growth of WO3 Photoanode under Various pH Conditions for Efficient Photoelectrochemical Performance. *Nanomaterials* **2024**, *14* (1), 8.
(68) Chacón, C.; Rodríguez-Pérez, M.; Oskam, G.; Rodríguez-Gattorno, G. Synthesis and characterization of WO3 polymorphs: Monoclinic, orthorhombic and hexagonal structures. *J. Mater. Sci.: Mater. Electron.* **2015**, *26* (8), 5526−5531.
(69) Li, Y.; Ma, Y.; Zhang, Y.; Wang, X.; Bai, F. Preparation of N-acetyl-para-aminophenol via a flow route of a clean amination and acylation of p-nitrophenol catalyzing by core-shell Cu2O@CeO2. *Arabian J. Chem.* **2020**, *13* (12), 8613−8625.
(70) Călinescu, O.; Badea, I. A.; Vlădescu, L.; Meltzer, V.; Pincu, E. HPLC Separation of Acetaminophen and its Impurities Using A Mixed-mode Reversed-Phase/Cation Exchange Stationary Phase. *J. Chromatogr. Sci.* **2012**, *50* (4), 335−342.
(71) Kianfar, A. H.; Arayesh, M. A. Synthesis, characterization and investigation of photocatalytic and catalytic applications of Fe3O4/TiO2/CuO nanoparticles for degradation of MB and reduction of nitrophenols. *J. Environ. Chem. Eng.* **2020**, *8* (1), 103640.
(72) Nekoeinia, M.; Yousefinejad, S.; Hasanpour, F.; Yousefian-Dezaki, M. Highly efficient catalytic degradation of p-nitrophenol by Mn3O4.CuO nanocomposite as a heterogeneous fenton-like catalyst. *J. Exp. Nanosci.* **2020**, *15* (1), 322−336.
(73) Varshney, S.; Bar-Ziv, R.; Zidki, T. On the Remarkable Performance of Silver-based Alloy Nanoparticles in 4-Nitrophenol Catalytic Reduction. *ChemCatchem* **2020**, *12* (18), 4680−4688.
(74) Geng, L.; An, S.; Wang, X.; Chen, J.; Liu, Z.; Zhang, X.; Zhang, D.-S.; Zhang, Y.-Z.; Wågberg, T.; Hu, G. Valence-mixed CuOx-nanoparticles anchored biomass-based carbon nanofiber for boosting toxic nitroarenes reduction: Synthesis, kinetics, and mechanisms. *J. Environ. Chem. Eng.* **2022**, *10* (6), 108689.
(75) Da'na, E.; Taha, A.; El-Aassar, M. R. Catalytic Reduction of p-Nitrophenol on MnO2/Zeolite −13X Prepared with Lawsonia inermis Extract as a Stabilizing and Capping Agent. *Nanomaterials* **2023**, *13* (4), 785.
(76) Nguyen, T. B.; Huang, C. P.; Doong, R.-A. Enhanced catalytic reduction of nitrophenols by sodium borohydride over highly recyclable Au@graphitic carbon nitride nanocomposites. *Appl. Catal., B* **2019**, *240*, 337−347.
(77) Shpak, A. P.; Korduban, A. M.; Medvedskij, M. M.; Kandyba, V. O. XPS studies of active elements surface of gas sensors based on WO3−x nanoparticles. *J. Electron Spectrosc. Relat. Phenom.* **2007**, *156−158*, 172−175.
(78) Darmawi, S.; Burkhardt, S.; Leichtweiss, T.; Weber, D. A.; Wenzel, S.; Janek, J.; Elm, M. T.; Klar, P. J. Correlation of electrochromic properties and oxidation states in nanocrystalline tungsten trioxide. *Phys. Chem. Chem. Phys.* **2015**, *17* (24), 15903−15911.
(79) Brady, R. L.; Southmayd, D.; Contescu, C.; Zhang, R.; Schwarz, J. A. Surface area determination of supported oxides: WO3/Al2O3. *J. Catal.* **1991**, *129* (1), 195−201.
(80) Zumreoglu-Karan, B.; Kose, D. A. Boric acid: A simple molecule of physiologic, therapeutic and prebiotic significance. *Pure Appl. Chem.* **2015**, *87* (2), 155−162.

https://doi.org/10.1021/acsomega.4c08455
ACS Omega 2025, 10, 10878−10890

(81) Badea, I. A.; Axinte, L.; Vladescu, L. Monitoring of aminophenol isomers in surface water samples using a new HPLC method. *Environ. Monit. Assess.* **2013**, *185* (3), 2367−2375.
(82) Ahmaruzzaman, M.; Mishra, S. R.; Gadore, V.; Yadav, G.; Roy, S.; Bhattacharjee, B.; Bhuyan, A.; Hazarika, B.; Darabdhara, J.; Kumari, K. Phenolic compounds in water: From toxicity and source to sustainable solutions − An integrated review of removal methods, advanced technologies, cost analysis, and future prospects. *J. Environ. Chem. Eng.* **2024**, *12* (3), 112964.

https://doi.org/10.1021/acsomega.4c08455
ACS Omega 2025, 10, 10878−10890